

Synthesis, Characterization, Photophysical and
Computational Study of Schiff Base Ligands and Their
Zn(II) Complexes

By

Naser Eltahir Eltayeb Taha

Thesis submitted in fulfillment of the requirements for

the degree of

Doctor of Philosophy

Universiti Sains Malaysia

August 2009

Dedication

To

My Parents

Eltaher Eltayeb Taha

&

Fatima Obaid Taha

ACKNOWLEDGMENTS

Since my first step in life till now a lot of people guide me through my education journey, my parents, my teachers in preschool, at primary school, at intermediate school, at secondary school, my lecturers at university, my supervisor in master degree and my PhD supervisors. So many people have helped me along this journey. It is impossible to name everyone whose effort has allowed me to achieve my goals and dreams.

I would like to take this opportunity to acknowledge people who have helped me in a number of ways to make this dissertation a reality. First, I would like to sincerely thank my main supervisor Prof. Teoh Siang Guan, and my co-supervisor, Dr. Rohana Adnan for their constant support and encouragement. I have learned a lot from them as supervisors as well as friends.

I would like to thank the financial support from International University of Africa, Sudan. I gratefully acknowledge the School of Chemical Sciences, USM for providing all the necessary facilities and equipments, and acknowledge the Universiti Sains Malaysia for financially supporting this work.

I would like to thank Prof. H. K. Fun and his students, Mohd Mustaqim Rosli, Shealin Ng and Jeannie Bee-Jan Teh for their helps in solving crystal structures. I would also like to thank Prof. Bohari M. Yamin (UKM), Prof. Kamarul Azizi (USM), for their help. I would also like to thank Ms. Seo-Hoon Goh (Osram) for her help.

Many friends as well as coworkers have helped me during my graduate work. I would like to thank Dr. Adil Elhag for his help in the processing my application for admission and his company during my research journey. I would like to thank my friends Dr. Abdalla, Mr. Abdallsalam, Mr. Aw yong, Dr. Aslam and Dr. Imtiyaz.

I would like to acknowledge my colleagues at International University of Africa, Dr. Shakh Idres, Prof. M. Ali Hussain, Mr. Mahmoud, Ibraheem, Abuzaid, Shingir Abuelresh and Alzaki who have encouraged me to pursue higher studies. I would like to thank the members of the Sudanese family at Universiti Sains Malaysia, Penang.

I would like to thank my parents who have always supported all my decisions and have been a source of constant energy to me. I would also like to thank my brothers and sisters, Qasim, Yasir, Eltayeb, Ahmed, Abeer and Areej whose encouragement has always kept me going.

Last but not least I would like to extend a special thanks to my wife, Ishraga and my son, Abdelmoniem, who have been here through all my happiness and sadness and constantly encourage me to achieve my higher dreams.

TABLE OF CONTENTS

| | |
|--|-------|
| Acknowledgement | ii |
| Tables of Contents | iv |
| List of Tables | xi |
| List of Figures | xv |
| List of Abbreviations | xxvi |
| Abstrak | xxvii |
| Abstract | xxix |
| | |
| Chapter One – Introduction | |
| 1.1 General Introduction | 1 |
| 1.2 Theoretical Background | 2 |
| 1.2.1 A Brief History of Luminescence | 2 |
| 1.2.2 Definition of Luminescence | 3 |
| 1.2.3 The Importance of the Photoluminescence and Electroluminescence | 7 |
| 1.3 Introduction to Computational Chemistry | 8 |
| 1.3.1 The Uses of Computational Chemistry | 9 |
| 1.3.2 The Tools of Computational Chemistry | 9 |
| 1.4 Background and Literature Review for Schiff Bases | 14 |
| 1.4.1 Definition | 14 |
| 1.4.2 Preparation of Schiff Bases | 14 |
| 1.4.3 Reaction Mechanism | 15 |
| 1.4.4 Schiff Base as Coordinating Ligands | 16 |
| 1.4.5 Applications of Schiff Bases and Their Complexes | 17 |

| | | |
|-------------------------------|---|----|
| 1.5 | Background and Literature Review for Zinc Complexes | 18 |
| 1.5.1 | Coordination Geometry of Zinc Complexes | 19 |
| 1.5.2 | Zinc in Biology | 20 |
| 1.5.3 | The Photophysical Properties of the Schiff Base-Zn(II) Complexes | 21 |
| 1.6 | Scope of the Thesis | 26 |
| 1.7 | Objectives of the Thesis | 26 |
| 1.8 | Organization of the Work | 27 |
| Chapter Two- Experimental | | |
| 2.1 | Materials | 28 |
| 2.2 | Synthetic Procedure for the Schiff Base Ligands | 28 |
| 2.2.1 | General Procedure for the Synthesis of Ligands | 28 |
| 2.2.2 | Synthesis of 2,2'-{1,2-phenylenebis[nitrilo methylidene]}diphenol (SB1) | 28 |
| 2.2.3 | Synthesis of 3,3'-{1,2-phenylenebis[nitrilomethylidene]} dibenzene-1,2-diol (SB2) | 29 |
| 2.2.4 | Synthesis of 4,4'-{1,2-phenylenebis[nitrilomethylidene]} dibenzene-1,3-diol (SB3) | 29 |
| 2.2.5 | Synthesis of 2,2'-{1,2-phenylenebis[nitrilomethylidene]} dibenzene-1,4-diol (SB4) | 30 |
| 2.2.6 | Synthesis of 6,6'-Dimethoxy-2,2'-[1,2-phenylenebis (nitrilomethylidene)]diphenol (SB5) | 31 |

| | | |
|--------|--|----|
| 2.2.7 | Synthesis of 5,5'-Dimethoxy-2,2'-[1,2-phenylenebis (nitrilomethylidyne)]diphenol (SB6) | 31 |
| 2.2.8 | Synthesis of 4,4'-Dimethoxy-2,2'-[1,2-phenylenebis (nitrilomethylidyne)]diphenol (SB7) | 32 |
| 2.2.9 | Synthesis of 6,6'-Dimethyl-2,2'-[1,2-phenylenebis (nitrilomethylidyne)]diphenol (SB8) | 32 |
| 2.2.10 | Synthesis of 5,5'-Dimethyl-2,2'-[1,2-phenylenebis (nitrilomethylidyne)] diphenol (SB9) | 33 |
| 2.2.11 | Synthesis of 4,4'-Dimethyl-2,2'-[1,2-phenylenebis (nitrilomethylidyne)] diphenol (SB10) | 33 |
| 2.2.12 | Synthesis of 4,4'-Dibromo-2,2'-[1,2-phenylenebis (nitrilomethylidyne)] diphenol (SB11) | 33 |
| 2.2.13 | Synthesis of 4,4'-Dichloro-2,2'-[1,2-phenylenebis (nitrilomethylidyne)] diphenol (SB12) | 34 |
| 2.2.14 | Synthesis of 4,4',6,6'-Tetra- <i>tert</i> -butyl-2,2'-[1,2-phenylenebis (nitrilometh -ylidyne)]diphenol (SB13) | 34 |
| 2.2.15 | Synthesis of 6,6'-Di- <i>tert</i> -butyl-2,2'-[1,2-phenylenebis (nitrilomethylidyne)] diphenol (SB14) | 35 |
| 2.3 | Synthetic Procedures for The Schiff Base-Zn(II) Complexes | 35 |
| 2.3.1 | General Procedure for the Synthesis of Zn(II) Complexes | 35 |
| 2.3.2 | Synthesis of Aqua{2,2'-[1,2-phenylenebis (nitrilomethylidyne)] diphenolato- $\kappa^4 O,N,N',O'$ }zinc(II) (Zn1) | 36 |
| 2.3.3 | Synthesis of an octanuclear zinc(II) complex with 6,6'-dihyd roxy-2,2'-[1,2-phenylenebis(nitrilomethylidyne)] diphenol (Zn2) | 36 |

| | | |
|--------|---|----|
| 2.3.4 | Synthesis of Aqua{5,5'-dihydroxy-2,2'-[1,2-phenylenebis (nitrilomethylidyne)] diphenolato- $\kappa^4 O,N,N',O'$ } zinc(II) (Zn3) | 37 |
| 2.3.5 | Synthesis of Aqua{4,4'-dihydroxy-2,2'-[1,2-phenylenebis (nitrilomethylidyne)] diphenolato- $\kappa^4 O,N,N',O'$ } zinc(II) (Zn4) | 37 |
| 2.3.6 | Synthesis of Aqua{6,6'-dimethoxy-2,2'-[1,2-phenylenebis (nitrilomethylidyne)] diphenolato- $\kappa^4 O,N,N',O'$ } zinc(II) (Zn5) | 38 |
| 2.3.7 | Synthesis of Aqua{5,5'-dimethoxy-2,2'-[1,2-phenylenebis (nitrilomethylidyne)] diphenolato- $\kappa^4 O,N,N',O'$ } zinc(II) (Zn6) | 39 |
| 2.3.8 | Synthesis of Aqua{4,4'-dimethoxy-2,2'-[1,2-phenylenebis (nitrilomethylidyne)]diphenolato- $\kappa^4 O,N,N',O'$ } zinc(II) (Zn7) | 39 |
| 2.3.9 | Synthesis of Aqua{6,6'-dimethyl-2,2'-[1,2-phenylenebis (nitrilomethylidyne)] diphenolato- $\kappa^4 O,N,N',O'$ } zinc(II) (Zn8) | 40 |
| 2.3.10 | Synthesis of Aqua{5,5'-dimethyl-2,2'-[1,2-phenylenebis (nitrilomethylidyne)]diphenolato- $\kappa^4 O,N,N',O'$ } zinc(II) (Zn9) | 40 |
| 2.3.11 | Synthesis of Aqua{4,4'-dimethyl-2,2'-[1,2-phenylenebis (nitrilomethylidyne)]diphenolato- $\kappa^4 O,N,N',O'$ } zinc(II) (Zn10) | 41 |
| 2.3.12 | Synthesis of Aqua{4,4'-dibromo-2,2'-[1,2-phenylenebis (nitrilomethylidyne)]diphenolato- $\kappa^4 O,N,N',O'$ } zinc(II) (Zn11) | 42 |
| 2.3.13 | Synthesis of Aqua{4,4'-dichloro-2,2'-[1,2-phenylenebis (nitrilomethylidyne)]diphenolato- $\kappa^4 O,N,N',O'$ } zinc(II) (Zn12) | 42 |
| 2.3.14 | Synthesis of (Ethanol- κO) {4,4',6,6'-Tetra- <i>tert</i> -butyl-2,2'- [1,2-phenylene -bis(nitrilomethylidyne)] diphenolato- $\kappa^4 O,N,N',O'$ } zinc(II) (Zn13) | 43 |

| | | |
|---|---|----|
| 2.3.15 | Synthesis of (Acetone- κO){6,6'-di- <i>tert</i> -butyl-2,2'-[1,2-phenylenebis (nitrilomethylidyne)] diphenolato- $\kappa^4 O,N,N',O'$ }zinc(II) (Zn14) | 43 |
| 2.4 | Physical measurement | 45 |
| 2.4.1 | Elemental Analysis | 45 |
| 2.4.2 | Infrared Measurement | 45 |
| 2.4.3 | UV-Vis Measurement | 45 |
| 2.4.4 | Fluorescence Measurement | 45 |
| 2.4.5 | Photoluminescence Measurements in Solid State | 46 |
| 2.4.6 | X-Ray Crystallography | 47 |
| 2.4.7 | Thermal Analysis | 47 |
| 2.5 | Computational Methods | 47 |
| 2.6 | Fabrication of OLED device with compound Zn13 | 48 |
| Chapter Three – Results and Discussion of Schiff Base Ligands | | |
| 3.1 | Synthesis and Characterization | 49 |
| 3.2 | FT-IR Spectroscopy | 50 |
| 3.3 | X-Ray Crystallographic Analyses | 55 |
| 3.3.1 | X-Ray Crystallographic Analysis of SB2 | 55 |
| 3.3.2 | X-Ray Crystallographic Analysis of SB3 | 59 |
| 3.3.3 | X-Ray Crystallographic Analysis of SB4 | 63 |
| 3.3.4 | X-Ray Crystallographic Analysis of SB5 | 67 |
| 3.3.5 | X-Ray Crystallographic Analysis of SB6 | 71 |
| 3.3.6 | X-Ray Crystallographic Analysis of SB7 | 75 |
| 3.3.7 | X-Ray Crystallographic Analysis of SB8 | 79 |

| | | |
|---|---|-----|
| 3.3.8 | X-Ray Crystallographic Analysis of SB9 | 83 |
| 3.3.9 | X-Ray Crystallographic Analysis of SB11 | 87 |
| 3.3.10 | X-Ray Crystallographic Analysis of SB12 | 91 |
| 3.3.11 | X-Ray Crystallographic Analysis of SB13 | 95 |
| 3.3.12 | X-Ray Crystallographic Analysis of SB14 | 99 |
| 3.4 | Photophysical Properties | 103 |
| 3.4.1 | Absorption Spectra of Schiff Base Ligands in Solution | 104 |
| 3.4.2 | Absorption Spectra of Schiff Base Ligands in Solid State | 107 |
| 3.4.3 | Fluorescence Emission Spectra of Schiff Base Ligands in Solutions | 109 |
| 3.4.4 | Fluorescence Emission Spectra of Schiff base Ligands in Solid State | 113 |
| 3.5 | Molecular Orbital Calculations | 115 |
| 3.5.1 | Molecular Geometry Optimization | 115 |
| 3.5.2 | Molecular Orbitals Analyses | 119 |
| 3.5.3 | Molecular Orbitals Energies | 123 |
| 3.5.4 | Comparison of Electronic Spectra | 124 |
| Chapter Four – Results and Discussion of Schiff Base-Zn(II) Complexes | | |
| 4.1 | Synthesis and Characterization | 127 |
| 4.2 | FT-IR Spectroscopy | 129 |
| 4.3 | X-Ray Crystallographic Analyses | 133 |
| 4.3.1 | X-Ray Crystallographic Analysis of Zn1 | 133 |
| 4.3.2 | X-Ray Crystallographic Analysis of Zn2 | 137 |
| 4.3.3 | X-Ray Crystallographic Analysis of Zn3 | 143 |

| | | |
|--------|--|-----|
| 4.3.4 | X-Ray Crystallographic Analysis of Zn7 | 147 |
| 4.3.5 | X-Ray Crystallographic Analysis of Zn8 | 151 |
| 4.3.6 | X-Ray Crystallographic Analysis of Zn10 | 155 |
| 4.3.7 | X-Ray Crystallographic Analysis of Zn11 | 159 |
| 4.3.8 | X-Ray Crystallographic Analysis of Zn12 | 163 |
| 4.3.9 | X-Ray Crystallographic Analysis of Zn13 | 167 |
| 4.3.10 | X-Ray Crystallographic Analysis of Zn14 | 171 |
| 4.4 | Photophysical Properties | 175 |
| 4.4.1 | Absorption Spectra of Schiff Base-Zn(II) Complexes in Solution | 175 |
| 4.4.2 | Absorption Spectra of Schiff Base-Zn(II) Complexes in Solid State | 178 |
| 4.4.3 | Fluorescence Emission Spectra of Schiff Base-Zn(II) Complexes in Solution | 180 |
| 4.4.4 | Fluorescence Emission Spectra of Schiff base-Zn(II) Complexes in Solid State | 184 |
| 4.5 | Molecular Orbital Calculations | 186 |
| 4.5.1 | Molecular Geometry Optimization | 187 |
| 4.5.2 | Molecular Orbitals Analyses | 190 |
| 4.5.3 | Molecular Orbitals energies | 194 |
| 4.5.4 | Comparison of Electronic Spectra | 196 |
| 4.6 | Thermal Properties | 198 |
| 4.6.1 | Thermogravimetric Analyses | 198 |
| 4.6.2 | Differential Scanning Calorimetry | 199 |

| | | |
|--|--|-----|
| 4.7 | Attempt fabrication of OLED device with compound Zn13 | 200 |
| Chapter Five – Summary and Conclusions | | |
| 5.1 | Summary | 201 |
| 5.2 | Conclusions | 202 |
| 5.3 | Suggestions for Future Research | 206 |
| | References | 207 |
| | Appendixs | |
| | Appendix A: Computational and Crystallographic Data for Schiff Base Ligands. | 221 |
| | Appendix B: Computational and Crystallographic Data for Schiff Base-Zn(II) complexes. | 261 |
| | Appendix C: Thermogravimetric Data for Schiff Base-Zn(II) complexes. | 301 |
| | Appendix D: Differential Scanning Calorimetric Data for Schiff Base- Zn(II) complexes | 308 |
| | List of Publications | 315 |

LIST OF TABLES

| | | |
|------------|--|-----|
| Table 3.1 | The crystal data and structure refinement parameters for SB2 ligand. | 56 |
| Table 3.2 | The crystal data and structure refinement parameters for SB3 ligand. | 60 |
| Table 3.3 | The crystal data and structure refinement parameters for SB4 ligand. | 64 |
| Table 3.4 | The crystal data and structure refinement parameters for SB5 ligand. | 68 |
| Table 3.5 | The crystal data and structure refinement parameters for SB6 ligand. | 72 |
| Table 3.6 | The crystal data and structure refinement parameters for SB7 ligand. | 76 |
| Table 3.7 | The crystal data and structure refinement parameters for SB8 ligand. | 80 |
| Table 3.8 | The crystal data and structure refinement parameters for SB9 ligand. | 84 |
| Table 3.9 | The crystal data and structure refinement parameters for SB11 ligand. | 88 |
| Table 3.10 | The crystal data and structure refinement parameters for SB12 ligand. | 92 |
| Table 3.11 | The crystal data and structure refinement parameters for SB13 ligand. | 96 |
| Table 3.12 | The crystal data and structure refinement parameters for SB14 ligand. | 100 |

| | | |
|------------|---|-----|
| Table 3.13 | Absorption and fluorescence of Schiff base ligands in DMF. | 103 |
| Table 3.14 | Comparison of selected bond lengths (Å), bond angles (°) and dihedral angles (°) from calculated optimized geometry and X-ray crystallographic studies of the ligand SB7. | 116 |
| Table 3.15 | HOMO and LUMO energies and band gap of Schiff base ligands. | 123 |
| Table 3.16 | Electronic absorption spectra values calculated by ZINDO/S method along with the transition assignment for SB7 ligand. | 126 |
| Table 4.1 | The crystal data and structure refinement parameters for Zn1 complex. | 134 |
| Table 4.2 | The crystal data and structure refinement parameters for Zn2 complex. | 139 |
| Table 4.3 | The crystal data and structure refinement parameters for Zn3 complex. | 144 |
| Table 4.4 | The crystal data and structure refinement parameters for Zn7 complex. | 148 |
| Table 4.5 | The crystal data and structure refinement parameters for Zn8 complex. | 152 |
| Table 4.6 | The crystal data and structure refinement parameters for Zn10 complex. | 156 |
| Table 4.7 | The crystal data and structure refinement parameters for Zn11 complex | 160 |
| Table 4.8 | The crystal data and structure refinement parameters for Zn12 complex. | 164 |

| | | |
|------------|--|-----|
| Table 4.9 | The crystal data and structure refinement parameters for Zn13 complex. | 168 |
| Table 4.10 | The crystal data and structure refinement parameters for Zn14 complex. | 172 |
| Table 4.11 | Absorption and fluorescence of Schiff base-Zn(II) complexes in DMF. | 175 |
| Table 4.12 | Comparison of selected bond lengths (Å), bond angles (°) and dihedral angles (°) from the optimized geometry and X-ray crystallographic data of the complex Zn3. | 187 |
| Table 4.13 | HOMO and LUMO energies and band gap of Zn(II) complexes. | 195 |
| Table 4.14 | Electronic absorption spectra values calculated by ZINDO/S method along with the transition assignment for Zn3 complex. | 197 |

LIST OF FIGURES

| | | |
|----------|---|----|
| Fig. 1.1 | Jablonski diagram (Chasteen, 1995). | 5 |
| Fig. 1.2 | Mechanism of Condensation of Carbonyl Compounds with Amines (Borisova <i>et al.</i> , 2007). | 16 |
| Fig. 3.1 | Synthetic route and structures for Schiff base ligands, SB1-SB14. | 50 |
| Fig. 3.2 | FTIR spectra for Schiff base ligands SB1-SB4. | 52 |
| Fig. 3.3 | FTIR spectra for Schiff base ligands SB5-SB9. | 53 |
| Fig. 3.4 | FTIR spectra for Schiff base ligands SB11-SB14. | 54 |
| Fig. 3.5 | The structure of SB2 ligand, showing 50% probability displacement ellipsoids and atomic numbering. For clarity, the solvent molecules have been omitted. | 57 |
| Fig. 3.6 | The crystal packing of SB2, viewed approximately along the <i>b</i> axis. | 58 |
| Fig. 3.7 | The asymmetric unit of SB3, showing 50% probability displacement ellipsoids and the atomic numbering. Intramolecular O—H...N, N—H...O and N—H...N hydrogen bonds are drawn as dashed lines. | 61 |
| Fig. 3.8 | The crystal packing of SB3, viewed along the <i>a</i> axis, showing the molecular chains along the <i>b</i> axis. Hydrogen bonds are drawn as dashed lines. | 62 |
| Fig. 3.9 | The asymmetric unit of SB4, showing 50% probability displacement ellipsoids and the atomic numbering. Hydrogen bonds are drawn as dashed lines. | 65 |

| | | |
|-----------|---|----|
| Fig. 3.10 | The crystal packing of SB4, viewed along the <i>c</i> axis, showing the molecular chains along the <i>b</i> axis. Hydrogen bonds are drawn as dashed lines. | 66 |
| Fig. 3.11 | The asymmetric unit of SB5, showing 50% probability displacement ellipsoids and the atomic numbering. Hydrogen bonds are drawn as dashed lines. | 69 |
| Fig. 3.12 | The crystal packing of SB5, viewed along the <i>a</i> axis. Hydrogen bonds are drawn as dashed lines. | 70 |
| Fig. 3.13 | The asymmetric unit of SB6, showing 50% probability displacement ellipsoids and the atomic numbering. Hydrogen bonds were drawn as dashed lines. | 73 |
| Fig. 3.14 | The crystal packing of SB6, viewed along the <i>a</i> axis. Hydrogen bonds were drawn as dashed lines. | 74 |
| Fig. 3.15 | The asymmetric unit of SB7, showing 50% probability displacement ellipsoids and the atomic numbering. Hydrogen bonds were drawn as dashed lines. | 77 |
| Fig. 3.16 | The crystal packing of SB7, viewed along the <i>b</i> axis. Hydrogen bonds were drawn as dashed lines. | 78 |
| Fig. 3.17 | The molecular structure of SB8, showing 50% probability displacement ellipsoids and the atomic numbering. Hydrogen bonds are shown as dashed lines. | 81 |
| Fig. 3.18 | The crystal packing of SB8, viewed down the <i>b</i> axis. Hydrogen bonds are shown as dashed lines. | 82 |

| | | |
|-----------|--|-----|
| Fig. 3.19 | The molecular structure of SB9, showing 50% probability displacement ellipsoids and the atomic numbering. Hydrogen bonds are shown as dashed lines. | 85 |
| Fig. 3.20 | The crystal packing of SB9, viewed down the <i>a</i> axis. H atoms not involved in intermolecular hydrogen bonding (dashed lines) have been omitted. | 86 |
| Fig. 3.21 | The molecular structure of SB11, showing 50% probability displacement ellipsoids and the atomic numbering. Hydrogen bonds are shown as dashed lines. | 89 |
| Fig.3.22 | The crystal packing of SB11, viewed down the <i>a</i> axis. Hydrogen bonds are shown as dashed lines. | 90 |
| Fig. 3.23 | The molecular structure of SB12, showing 50% probability displacement ellipsoids and the atomic numbering. Hydrogen bonds are shown as dashed lines. | 93 |
| Fig. 3.24 | The crystal packing of SB12, viewed down the <i>a</i> axis. Hydrogen bonds are shown as dashed lines. | 94 |
| Fig. 3.25 | The asymmetric unit of SB13, showing 50% probability displacement ellipsoids and the atomic numbering. Hydrogen bonds were drawn as dash lines. | 97 |
| Fig. 3.26 | The crystal packing of SB13, viewed along the <i>c</i> axis. For clarify, the molecules of acetone were omitted. | 98 |
| Fig. 3.27 | The asymmetric unit of SB14, showing 50% probability displacement ellipsoids and the atomic numbering. Hydrogen bonds were drawn as dashed lines. | 101 |

| | | |
|-----------|---|-----|
| Fig. 3.28 | The crystal packing of SB14, viewed along the <i>c</i> axis | 102 |
| Fig. 3.29 | The absorption spectra of ligands SB1-SB4 in DMF at room temperature. | 105 |
| Fig. 3.30 | The absorption spectra of ligands SB5-SB9 in DMF at room temperature. | 106 |
| Fig. 3.31 | The absorption spectra of ligands SB11-SB14 in DMF at room temperature. | 106 |
| Fig. 3.32 | The absorption spectra of ligands SB1-SB4 in solid state at room temperature. | 107 |
| Fig. 3.33 | The absorption spectra of ligands SB5-SB9 in solid state at room temperature. | 108 |
| Fig. 3.34 | The absorption spectra of ligands SB11-SB14 in solid state at room temperature. | 108 |
| Fig. 3.35 | The emission spectra of ligands SB1-SB4 in DMF at room temperature. | 111 |
| Fig. 3.36 | The emission spectra of ligands SB5-SB9 in DMF at room temperature. | 112 |
| Fig. 3.37 | The emission spectra of ligands SB11-SB14 in DMF at room temperature. | 112 |
| Fig. 3.38 | The emission spectra of ligands SB1-SB4 in solid state at room temperature. | 113 |
| Fig. 3.39 | The emission spectra of ligands SB5-SB8 in solid state at room temperature. | 114 |
| Fig. 3.40 | The emission spectra of ligands SB9 and SB11-SB14 in solid state at room temperature. | 114 |

| | | |
|-----------|---|-----|
| Fig. 3.41 | Optimized structure of SB7 ligand and its atomic numbering. | 116 |
| Fig. 3.42 | Experimental X-ray versus theoretical PM6 bond lengths. | 117 |
| Fig. 3.43 | Experimental X-ray versus theoretical PM6 bond angles. | 118 |
| Fig. 3.44 | Experimental X-ray versus theoretical PM6 dihedral angles. | 118 |
| Fig. 3.45 | HOMO and LUMO of SB7 from the Hartee-Fock calculation at HF/6-31+G level. | 120 |
| Fig. 3.46 | Percent contributions to molecular orbitals of SB7 ligand. | 122 |
| Fig. 3.47 | Molecular orbital energies for the first eight HOMOs and LUMOs of SB1-SB7. | 124 |
| Fig. 3.48 | Comparison of calculated and experimental absorption for SB7 ligand. | 126 |
| Fig. 4.1 | Synthetic route and structures for Zn(II)-Schiff base complexes Zn1-Zn14. | 128 |
| Fig. 4.2 | FTIR spectra for Schiff base-Zn(II) complexes Zn1-Zn4. | 130 |
| Fig. 4.3 | FTIR spectra for Schiff base-Zn(II) complexes Zn5-Zn9. | 131 |
| Fig. 4.4 | FTIR spectra for Schiff base-Zn(II) complexes Zn10-Zn14. | 132 |
| Fig. 4.5 | The molecular structure of Zn1, showing 50% probability displacement ellipsoids and the atomic numbering. The dashed line indicates the intramolecular hydrogen bond. | 135 |
| Fig. 4.6 | The crystal packing of Zn1, viewed down the <i>a</i> axis. The intermolecular C-H...O hydrogen bonds are shown as dashed lines. H atoms not involved in hydrogen bonding have been omitted. | 136 |
| Fig. 4.7 | The asymmetric unit of Zn2, displacement ellipsoids are drawn at the 50% probability level. | 140 |

| | | |
|-----------|--|-----|
| Fig. 4.8 | The molecular structure of the Zn ₂ , Showing 50% probability displacement ellipsoids and the atomic numbering. H atoms of Zn(II) complex, DMSO and solvated water molecules have been omitted for clarity. | 141 |
| Fig. 4.9 | The crystal packing of Zn ₂ complex, viewed along the <i>c</i> axis, showing sheets parallel to the <i>ab</i> plane. Hydrogen bonds are shown as dashed lines. | 142 |
| Fig. 4.10 | The asymmetric unit of Zn ₃ complex, showing 50% probability displacement ellipsoids and the atomic numbering. Hydrogen bonds are drawn as dashed lines. | 145 |
| Fig. 4.11 | The crystal packing of Zn ₃ , viewed along the <i>a</i> axis. Hydrogen bonds are shown as dashed lines. | 146 |
| Fig. 4.12 | The asymmetric unit of Zn ₇ , Showing 50% probability ellipsoids and the atomic numbering. | 149 |
| Fig. 4.13 | The crystal packing of Zn ₇ , viewed along the <i>b</i> axis. Hydrogen bonds are shown as dashed lines. | 150 |
| Fig. 4.14 | The asymmetric unit of Zn ₈ , showing 50% probability displacement ellipsoids and the atomic numbering. | 153 |
| Fig. 4.15 | The crystal packing of Zn ₈ , viewed along the <i>b</i> axis. Only water and chloroform H atoms were drawn for clarify. Hydrogen bonds are shown as dash lines. | 154 |
| Fig. 4.16 | The asymmetric unit of Zn ₁₀ , showing 50% probability displacement ellipsoids and the atomic numbering. | 157 |
| Fig. 4.17 | The crystal packing of Zn ₁₀ , viewed along the <i>a</i> axis. Hydrogen bonds are shown as dashed lines. | 158 |

| | | |
|-----------|---|-----|
| Fig. 4.18 | The molecular structure of Zn11, showing 50% probability displacement ellipsoids and the atomic numbering. Intramolecular hydrogen bonds are shown as dashed lines. | 161 |
| Fig. 4.19 | The crystal packing of Zn11, viewed down the <i>b</i> axis. H atoms not involved in intermolecular hydrogen bonding have been omitted. | 162 |
| Fig. 4.20 | The asymmetric unit of Zn12, showing 60% probability displacement ellipsoids and the atomic numbering. | 165 |
| Fig. 4.21 | The crystal packing of Zn12, viewed along the <i>a</i> axis. Hydrogen bonds are shown as dashed lines. | 166 |
| Fig. 4.22 | The asymmetric unit of Zn13, showing 50% probability displacement ellipsoids and the atomic numbering. C-bound H atoms of Zn13 complex have been omitted for clarity. | 169 |
| Fig. 4.23 | The crystal packing of Zn13, viewed along the <i>b</i> axis. C-bound H atoms of the Zn13 complex have been omitted for clarity. Hydrogen bonds are shown as dashed lines. | 170 |
| Fig. 4.24 | The structure of Zn14, showing 50% probability displacement ellipsoids and the atomic numbering. | 173 |
| Fig. 4.25 | The crystal packing of Zn14, viewed approximately along the <i>b</i> axis. | 174 |
| Fig. 4.26 | The absorption spectra of complexes Zn1-Zn4 in DMF at room temperature. | 177 |
| Fig. 4.27 | The absorption spectra of complexes Zn5-Zn9 in DMF at room temperature. | 177 |

| | | |
|-----------|---|-----|
| Fig. 4.28 | The absorption spectra of complexes Zn10-Zn14 in DMF at room temperature. | 178 |
| Fig. 4.29 | The absorption spectra of complexes Zn1-Zn4 in solid state at room temperature. | 179 |
| Fig. 4.30 | The absorption spectra of complexes Zn5-Zn10 in solid state at room temperature. | 179 |
| Fig. 4.31 | The absorption spectra of complexes Zn11-Zn14 in solid state at room temperature. | 180 |
| Fig. 4.32 | The emission spectra of complexes Zn1-Zn4 in DMF at room temperature. | 183 |
| Fig. 4.33 | The emission spectra of complexes Zn5-Zn9 in DMF at room temperature. | 183 |
| Fig. 4.34 | The emission spectra of complexes Zn10-Zn14 in DMF at room temperature. | 184 |
| Fig. 4.35 | The emission spectra of complexes Zn1-Zn4 in solid state at room temperature. | 185 |
| Fig. 4.36 | The emission spectra of complexes Zn5-Zn10 in solid state at room temperature. | 185 |
| Fig. 4.37 | The emission spectra of complexes Zn11-Zn14 in solid state at room temperature. | 186 |
| Fig. 4.38 | Optimized structure of Zn3 complex and its atomic numbering. | 188 |
| Fig. 4.39 | Experimental X-ray versus theoretical PM6 bond lengths. | 188 |
| Fig. 4.40 | Experimental X-ray versus theoretical PM6 bond angles. | 189 |
| Fig. 4.41 | Experimental X-ray versus theoretical PM6 dihedral angles. | 189 |

| | | |
|-----------|--|-----|
| Fig. 4.42 | HOMO and LUMO of Zn3 complex from the Hartee-Fock calculation at HF/6-31+G level. | 191 |
| Fig. 4.43 | HOMO and LUMO of Zn4 complex from the Hartee-Fock calculation at HF/6-31+G level. | 191 |
| Fig. 4.44 | Percent contributions to molecular orbitals of Zn3 complex. | 192 |
| Fig. 4.45 | Molecular orbital energies for the first eight HOMOs and LUMOs of Zn1 and Zn3-Zn7 Complexes. | 195 |
| Fig. 4.46 | Comparison of calculated and experimental absorption for Zn3 complex. | 197 |
| Fig. 4.47 | TGA for Zn12 complex. | 198 |
| Fig. 4.48 | DSC for Zn12 complex. | 199 |
| Fig. 4.49 | Fabricated OLED device using Zn13 as emitting layer. | 200 |

LIST OF APPREVIATIONS

| | |
|-------|--|
| AAS | Atomic Absorption Spectroscopy |
| B3LYP | Becke, three-parameter, Lee-Yang-Parr |
| CIS | Configuration Interaction Singles |
| CT | Charge Transfer |
| DFT | Density Functional Theory |
| DMF | N,N-Dimethylformamide |
| FTIR | Fourier Transform Infrared |
| HF | Hartree-Fock |
| HOMO | Highest Occupied Molecular Orbital |
| INDO | Intermediate Neglect of Differential Overlap |
| ITO | Indium Tin Oxide |
| LED | Light Emitting Diodes |
| LUMO | Lowest Unoccupied Molecular Orbital |
| MO | Molecular Orbitals |
| MM | Molecular Mechanics |
| NDDO | Neglect of Diatomic Differential Overlap |
| OLED | Organic Light Emitting Diodes |
| Pedot | Poly(3,4-ethylenedioxythiophene) |
| PL | Photoluminescence |
| PM6 | Parameterization Method 6 |
| QSPR | Quantitative Structure-Property Relationship |
| SB1 | 2,2'-{1,2-phenylenebis[nitrilomethylylidene]}diphenol |
| SB2 | 3,3'-{1,2-phenylenebis[nitrilomethylylidene]} dibenzene-1,2-diol |
| SB3 | 4,4'-{1,2-phenylenebis[nitrilomethylylidene]} dibenzene-1,3-diol |

| | |
|---------|--|
| SB4 | 2,2'-{1,2-phenylenebis[nitrilomethylylidene]} dibenzene-1,4-diol |
| SB5 | 6,6'-Dimethoxy-2,2'-[1,2-phenylenebis (nitrilomethylidyne)] diphenol |
| SB6 | 5,5'-Dimethoxy-2,2'-[1,2-phenylenebis (nitrilomethylidyne)] diphenol |
| SB7 | 4,4'-Dimethoxy-2,2'-[1,2-phenylenebis (nitrilomethylidyne)] diphenol |
| SB8 | 6,6'-Dimethyl-2,2'-[1,2-phenylenebis (nitrilomethylidyne)] diphenol |
| SB9 | 5,5'-Dimethyl-2,2'-[1,2-phenylenebis (nitrilomethylidyne)] diphenol |
| SB10 | 4,4'-Dimethyl-2,2'-[1,2-phenylenebis (nitrilomethylidyne)] diphenol |
| SB11 | 4,4'-Dibromo-2,2'-[1,2-phenylenebis (nitrilomethylidyne)] diphenol |
| SB12 | 4,4'-Dichloro-2,2'-[1,2-phenylenebis (nitrilomethylidyne)] diphenol |
| SB13 | 4,4',6,6'-Tetra- <i>tert</i> -butyl-2,2'-[1,2-phenylenebis (nitrilometh - ylidyne)]diphenol |
| SB14 | 6,6'-Di- <i>tert</i> -butyl-2,2'-[1,2-phenylenebis (nitrilomethylidyne)] diphenol |
| SE | Semi-empirical |
| UV/Vis | Ultraviolet/Visible |
| ZINDO/S | Zerner's Intermediate Neglect of Differential Overlap |
| Zn1 | Aqua{2,2'-[1,2-phenylenebis(nitrilomethylidyne)] diphenolato- $\kappa^4 O, N, N', O'$ }zinc(II) |
| Zn2 | Octanuclear zinc(II) complex with 6,6'-dihydroxy-2,2'-[1,2- phenylenebis(nitrilomethylidyne)] diphenol |
| Zn3 | Aqua{5,5'-dihydroxy-2,2'-[1,2-phenylenebis (nitrilomethylidyne)] diphenolato- $\kappa^4 O, N, N', O'$ }zinc(II) |
| Zn4 | Aqua{4,4'-dihydroxy-2,2'-[1,2-phenylenebis (nitrilomethylidyne)] diphenolato- $\kappa^4 O, N, N', O'$ }zinc(II) |
| Zn5 | Aqua{6,6'-dimethoxy-2,2'-[1,2-phenylenebis (nitrilomethylidyne)] |

- diphenolato- $\kappa^4 O,N,N',O'$ }zinc(II)
- Zn6 Aqua{ 5,5'-dimethoxy-2,2'-[1,2-phenylenebis (nitrilomethylidyne)]
diphenolato- $\kappa^4 O,N,N',O'$ }zinc(II)
- Zn7 Aqua{ 4,4'-dimethoxy-2,2'-[1,2-phenylenebis
(nitrilomethylidyne)]diphenolato- $\kappa^4 O,N,N',O'$ }zinc(II)
- Zn8 Aqua{ 6,6'-dimethyl-2,2'-[1,2-phenylenebis (nitrilomethylidyne)]
diphenolato- $\kappa^4 O,N,N',O'$ }zinc(II)
- Zn9 Aqua{ 5,5'-dimethyl-2,2'-[1,2-phenylenebis
(nitrilomethylidyne)]diphenolato- $\kappa^4 O,N,N',O'$ }zinc(II)
- Zn10 Aqua{ 4,4'-dimethyl-2,2'-[1,2-phenylenebis (nitrilomethylidyne)]
diphenolato- $\kappa^4 O,N,N',O'$ }zinc(II)
- Zn11 Aqua{ 4,4'-dibromo-2,2'-[1,2-phenylenebis (nitrilomethylidyne)]
diphenolato- $\kappa^4 O,N,N',O'$ }zinc(II)
- Zn12 Aqua{ 4,4'-dichloro-2,2'-[1,2-phenylenebis (nitrilomethylidyne)]
diphenolato- $\kappa^4 O,N,N',O'$ }zinc(II)
- Zn13 (Ethanol- κO) { 4,4',6,6'-Tetra-*tert*-butyl-2,2'-[1,2-phenylene -
bis(nitrilomethylidyne)] diphenolato- $\kappa^4 O,N,N',O'$ }zinc(II)
- Zn14 (Acetone- κO) { 6,6'-di-*tert*-butyl-2,2'-[1,2-phenylenebis
(nitrilomethylidyne)] diphenolato- $\kappa^4 O,N,N',O'$ }zinc(II)

Sintesis, Pencirian, Fotofizikal dan Kajian Pengkompputeran Ligan Schiff Bes dan Kompleks Zn(II)nya

ABSTRAK

Ligan bes Schiff dan kompleks Zn(II)nya telah menunjukkan kebolehan yang baik untuk pelbagai aplikasi disebabkan sifat-sifat dalam keadaan asas dan terujanya yang menarik. Oleh yang demikian adalah penting untuk memahami kaedah bagi mengawal sifat-sifat fizik dan kimia sebatian ini bagi membolehkan sifat fotofiziknya diubah bersesuaian dengan aplikasi tertentu. Fokus kajian disertasi ini tertumpu kepada penyediaan dan pencirian pelbagai jenis ligan bes Schiff bersama kompleks Zn(II) serta mengkaji sifat-sifat fotofiziknya. Kajian ini dibahagikan kepada empat bahagian utama. Dalam bahagian pertama, empat belas ligan bes Schiff bersama kompleks Zn(II)nya telah disintesis dan dicirikan sepenuhnya menggunakan kaedah spektroskopi infra-merah (FTIR), analisis unsur, spektroskopi penyerapan atom (AAS) dan pembelauan sinar-X hablur tunggal. Di dalam bahagian kedua, sifat fotofizik sebatian ini dikaji dalam fasa cecair dan pepejal menggunakan kaedah spektroskopi ultraungu nampak dan pendarfluor. Seterusnya, sifat-sifat terma bes Schiff bersama kompleks Zn(II)nya diperolehi menggunakan kaedah analisis terma gravimetri (TGA) dan kalorimetri pembezaan pengimbasan (DSC). Di dalam bahagian ketiga, pengiraan berasaskan komputer telah dijalankan menggunakan kaedah semi empirik PM6 dan ZINDO/S. Ini adalah bertujuan untuk mengkaji kelakuan taburan elektron dan penyerapan optik sebatian-sebatian ini. Keputusan yang diperolehi daripada kaedah pengkompputeran adalah berpadanan dengan keputusan eksperimen dan ini menunjukkan bahawa kaedah ini adalah sesuai untuk merekabentuk sebatian pendarcahaya yang baru. Bahagian terakhir melibatkan

percubaan fabrikasi ke atas peranti diod pancaran cahaya organik (OLED). Kompleks Zn13 telah dipilih untuk fabrikasi kerana sebatian ini menunjukkan sifat pendarcahaya yang baik serta keterlarutan yang tinggi dalam pelarut organik. Peranti ini telah berjaya difabrikasi, bagaimanapun, jangka hayat peranti yang dihasilkan adalah singkat maka sifat-sifat lain bagi peranti ini tidak dapat ditentukan. Justeru beberapa langkah dicadangkan untuk mengoptimumkan peranti yang dihasilkan dan seterusnya meningkatkan jangka hayatnya. Berdasarkan kepada penemuan ini, dapat disimpulkan bahawa sintesis dengan menggunakan kaedah pengawalan ligan dapat menghasilkan bahan pendarcahaya dengan warna, jurang tenaga jalur optik dan kestabilan terma yang diinginkan. Kajian ini turut membuktikan kompleks Schiff bes bersama Zn(II) yang telah disintesis ini berkeupayaan untuk digunakan dalam aplikasi OLED.

Synthesis, Characterization, Photophysical and Computational Study of Schiff Base Ligands and Their Zn(II) Complexes

ABSTRACT

Schiff base ligands and their Zn(II) complexes have shown good potentials in a range of applications due to their interesting ground and excited state properties. It is therefore vital to understand how to control the physical and chemical properties of such compounds in order to be able to tune their photophysical properties according to application-specific requirements. This dissertation focuses on the synthesis, characterization and photophysical properties of a variety of Schiff base ligands and their Zn(II) complexes.

The work was divided into four main parts. In the first part, fourteen Schiff bases ligands and their Zn(II) complexes were synthesized and fully characterized using fourier transform infrared spectroscopy (FTIR), elemental analysis, atomic absorption spectroscopy (AAS) and X-ray single crystal diffractions.

In the second part, the photophysical properties of these compounds were investigated in both liquid and solid state using ultraviolet visible (UV/Vis) and fluorescence spectroscopy. Moreover, the thermal properties of the Schiff bases-Zn(II) complexes were studied using thermogravimetric analysis (TGA) and differential scanning calorimetry (DSC).

In the third part, computational calculations were performed using PM6 and ZINDO/S at semi-empirical level to study the optical absorption spectra of these compounds. The computational results give good agreement with the experimental findings, which indicate the usefulness of these calculations in the design of new luminescent compounds.

The final part of this work involved attempted fabrication of the organic light emitting diode (OLED) device. The Schiff base-Zn(II) complex, Zn13, was selected for OLED device fabrication due to its good luminescence properties and high solubility in organic solvents. The device was successfully fabricated, but due to its short lifetime we did not able to measure more of its properties. Further optimization of the device has to be carried out to enhance its lifetime.

Based on the findings we can suggest that new luminescent materials with desired color, thermal stability and optical band gap energy could be obtained by synthesis of specific ligands. It is envisaged that the new Schiff base-Zn(II) materials synthesized in the present work have potential for application as organic light emitting diodes (OLED).

Chapter One

Introduction

Introduction

1.1 General introduction

Photophysical properties of transition metal complexes is a field of considerable interest because a better understanding of the excited-state properties helps in the design of new molecules as fluorescent probes for sensing and highly luminescent materials, especially for organic light emitting devices. Compounds with extended π -systems, conjugated polymers, well defined oligomers have become an important class of electronic materials. The photophysics and photochemistry of luminescent transition metal ions coordinated by organic ligands have received widespread interest. In part, the interest stems from the applicability of metal complexes as photocatalysts (Yin and Moss, 1999), as photosensitizer material in solar energy conversion (Kalyanasundaram and Gratzel, 1998), in molecular diodes (Aoki *et al.*, 1999), as chemical sensors (Draxler *et al.*, 1995) or as biosensors (Holmlin *et al.*, 1999), and in supramolecular clusters that mimic biological light harvesting systems (Balzani *et al.*, 1998). Numerous optical spectroscopic studies have contributed in obtaining the information necessary for a better understanding of the structure and chemical bonding of the transition metal compounds (Glasbeek, 2001).

Schiff base complexes have been studied for their wide applications in various fields such as catalysis, as corrosion inhibitors and in biological field, etc. (Capape *et al.*, 2008; Keles *et al.*, 2008; El-tabl *et al.*, 2008; Aksuner *et al.*, 2008; Gupta and Sutar, 2008). However, the studies on their optical properties, such as fluorescence, are rare (Majumder *et al.*, 2006). Search on the keyword “Schiff base” in the SciFinder database results in 39894 articles, among them only 209 articles contain the keyword “luminescence”. Among these just 38 articles contain the keyword “Zinc” (SciFinder, 2008).

We have been interested in preparing Schiff bases and their zinc complexes in an effort to study the luminescence properties of these compounds. Study and design of fluorescence properties of the Schiff bases and their transition metal complexes might open up new path for further applications such as organic light emitting diodes (OLED), biosensors and probes. For the above mentioned reasons the synthesis and characterization of a series of Schiff base ligands and their zinc complexes and studies of their photophysical properties will be carried out. Computational calculations will be employed to study some molecular properties such as absorption, molecular orbital, molecular orbital energy for these compounds.

1.2 Theoretical Background

1.2.1 A brief History of Luminescence

Luminescence as a weak cold glow from rotting wood, certain insects, mushrooms, fish, microorganisms, sea alga, minerals, and polar lights has been known since ancient times. This interesting and initially mysterious phenomenon attracted the attention of many scientists during the last four centuries (Gribkovskii, 1998). Luminescence has been first observed in 1565 by Nicolás Monardes, who reported the blue colour that is observed from water extracts of the wood of a small tree, Coatli, (*Ligirium nephiticiem*) used in the Aztec culture to treat kidney maladies (Parola *et al.*, 2008). David Brewster noted the red emission from chlorophyll in 1833, and G. G. Stokes described the mechanism of the absorption and emission process in 1852, and formulated the first law in the history of luminescence (Guilbault *et. al*, 1973), Stokes' law, which states that the wavelength of the luminescence is greater than the wavelength of the exciting radiation. Stokes also named fluorescence after the mineral fluorspar (Latin fluo = to flow + spar = a rock), which exhibited a blue-white fluorescence. Phosphorescence dates back to the early

1500s, being so named after the Greek word for “light bearing” (Guilbault *et. al*, 1973).

1.2.2 Definition of Luminescence

Luminescence is an emission of ultraviolet, visible or infrared photons from an electronically excited species. The word luminescence, which comes from the Latin (*lumen* = light) was first introduced as *luminescenz* by the physicist and science historian Eilhardt Wiedemann in 1888, to describe ‘all those phenomena of light which are not solely conditioned by the rise in temperature’, as opposed to incandescence. Luminescence is cold light whereas incandescence is hot light (Valeur, 2002).

The various types of luminescence according to the mode of excitation (Valeur, 2002) are listed below:

- (i) Photoluminescence (fluorescence, phosphorescence, delayed fluorescence) when the system was excited by absorption of light (photons).
- (ii) Radioluminescence when the system was excited by ionizing radiation (X-rays, α , β and γ).
- (iii) Cathodoluminescence when the system was excited by cathode rays (electron beams).
- (iv) Electroluminescence when the system was excited by an electric field.
- (v) Thermoluminescence when the system was excited by heating after prior storage of energy (e.g. radioactive irradiation).
- (vi) Chemiluminescence when the system was excited by chemical process (e.g. oxidation).
- (vii) Bioluminescence when the system was excited by biochemical process.

(viii) Triboluminescence when the system was excited by frictional and electrostatic forces.

(ix) Sonoluminescence when the system excited by ultrasounds.

Luminescence is formally divided into two categories: fluorescence and phosphorescence depending on the nature of the excited state. In excited singlet states, the electron in the excited orbital is paired (by opposite spin) to the second electron in the ground-state orbital. Consequently, return to the ground state is spin allowed and occurs rapidly by emission of a photon. The emission rates of fluorescence are typically 10^{-8} s, so that a typical fluorescence lifetime is near 10 ns (10×10^{-9} s). Because of the short timescale of fluorescence, measurement of the time-resolved emission requires sophisticated optics and electronics (Lacowicz, 2006).

Phosphorescence is emission of light from triplet excited states, in which the electron in the excited state has the same spin orientation as the ground-state electron. Transitions to the ground state are forbidden and the emission rates are slow (10^{-3} to 10^0 s), so that phosphorescence lifetimes are typically milliseconds to seconds; however, longer lifetimes are possible. Following exposure to light, the phosphorescence substances glow for several minutes while the excited phosphors slowly return to the ground state. Phosphorescence is usually not seen in fluid solutions at room temperature. This is because there are many deactivation processes that compete with emission, such as non-radiative decay and quenching processes. It should be noted that the distinction between fluorescence and phosphorescence is not always clear. Transition metal–ligand complexes, which contain a metal and one or more organic ligands, display mix singlet–triplet states. These complexes display

intermediate lifetimes of hundreds of nanoseconds to several microseconds (Lacowicz, 2006).

Fluorescence is a type of photoluminescence that is generated when a photon of specific energy is absorbed by a molecule wherein an electron within the molecule is promoted from the ground state to an electronically excited state. The excited state can exist either as a singlet or triplet state. The singlet excited state occurs when the electron is paired with another electron of opposing spin. This is a quantum-mechanically allowed transition, and fluorescence emission occurs as a result of the spin-paired excited electron returning to the ground state. The triplet excited state occurs when the excited electron is of the same spin as the second electron in the pair, and upon relaxation, the electron must undergo a “spin-flip” to return to the singlet ground state. These processes are represented in the Jablonski diagram (Wang *et al.*, 2007). Processes which occur between the absorption and emission of light are usually illustrated by a Jablonski diagram. A typical Jablonski diagram is shown in Fig.1.1, below.

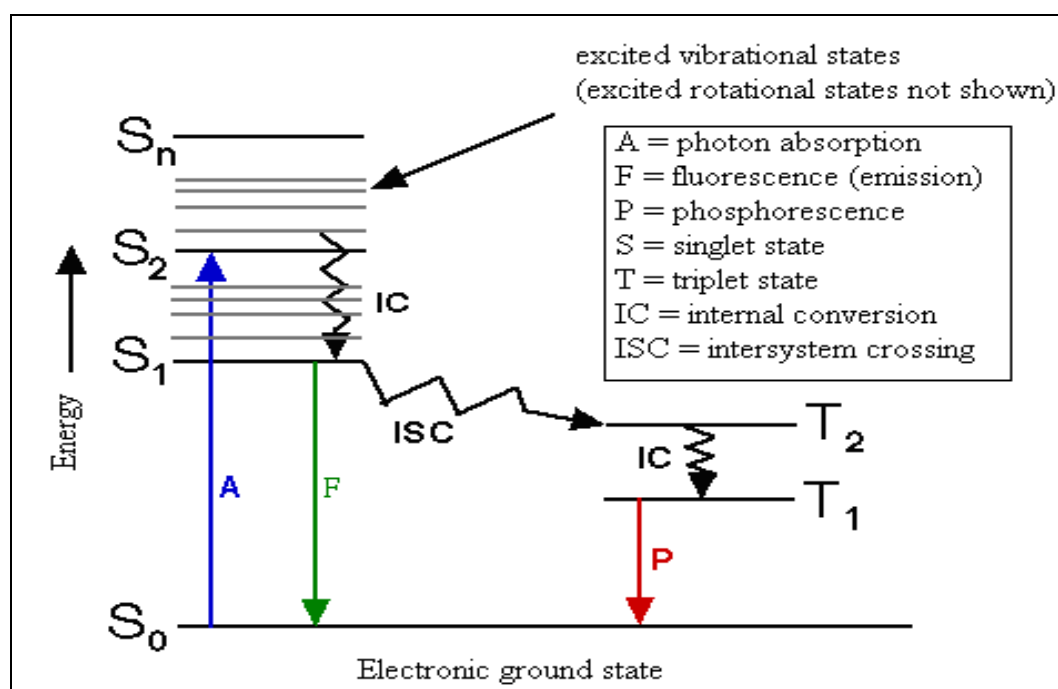


Fig. 1.1. Jablonski diagram (Chasteen, 1995).

The singlet ground, first, and second electronic states are depicted as S_0 , S_1 , and S_2 , respectively. At each of these electronic energy levels, the fluorophores can exist in a number of vibrational energy levels, depicted as 0, 1, 2, etc. The transitions between states are depicted as vertical lines to illustrate the instantaneous nature of light absorption. Transitions occur in about 10^{-15} s, a time too short for significant displacement of nuclei. This is referred as the Franck-Condon principle (Lacowicz, 2006)

Absorption and emission occur mostly from molecules with the lowest vibrational energy. The larger energy difference between the S_0 and S_1 excited states is too large for thermal population of S_1 . For this reason we use light and not heat to induce fluorescence. Following light absorption, several processes usually occur. A fluorophore is usually excited to some higher vibrational level of either S_1 or S_2 . With a few rare exceptions, molecules in condensed phases rapidly relax to the lowest vibrational level of S_1 . This process is called internal conversion and generally occurs within 10^{-12} s or less. Since fluorescence lifetimes are typically near 10^{-8} s, internal conversion is generally complete prior to emission. Hence, fluorescence emission generally results from a thermally equilibrated excited state, that is, the lowest energy vibrational state of S_1 . Return to the ground state typically occurs at a higher excited vibrational ground state level, which then quickly (10^{-12} s) reaches thermal equilibrium (Lacowicz, 2006).

An interesting consequence of emission to higher vibrational ground states is that the emission spectrum is typically a mirror image of the absorption spectrum. This similarity occurs because electronic excitation does not greatly alter the nuclear geometry. Hence the spacing of the vibrational energy levels of the excited state is similar to that of the ground state. As a result, the vibrational structures seen in the

absorption and the emission spectra are similar. Molecules in the S_1 state can also undergo a spin conversion to the first triplet state T_1 . Emission from T_1 is termed phosphorescence, and is generally shifted to longer wavelengths (lower energy) relative to the fluorescence. Conversion of S_1 to T_1 is called intersystem crossing. Transition from T_1 to the singlet ground state is forbidden, and as a result the rate constants for triplet emission are several orders of magnitude smaller than those for fluorescence. Molecules containing heavy atoms such as bromine and iodine are frequently phosphorescent. The heavy atoms facilitate intersystem crossing and thus enhance phosphorescence quantum yields (Lacowicz, 2006).

Emission from the triplet state results in phosphorescence. This is rarely seen for organic molecules in solution because these molecules are readily quenched by solution species before emission. However, emission from triplet states is found with metal chelates which have much shorter emission lifetimes than organic molecules (Bard, 2004).

1.2.3 The Importance of the Photoluminescence and Electroluminescence

The growing demand for photoluminescent and electroluminescent materials has stimulated much fundamental material research in both organic and inorganic syntheses. Transition metal complexes are finding broad potential applications in organic light-emitting diodes (Yersin, 2004; Tsuboyama *et al.*, 2003), light-emitting diodes, light-emitting electrochemical cell (Bolink, 2006), solar cells (Wong *et al.*, 2007) and sensors (Xu *et al.*, 1996; Takeuchi and Amao, 2005). Due to their desirable optical, electronic and mechanical properties, these compounds play an important role in developing semiconductors and optoelectronic devices.

1.3 Introduction to Computational Chemistry

The application of modern computational techniques to transition metals and organometallic chemistry has truly undergone a renaissance in the past few years. The last decade has witnessed the establishment of quantum chemical methods as a standard tool for quantitative calculations of transition metal compounds, after numerous theoretical studies have proven that the results obtained are highly accurate. The calculated data can be used to interpret experimental observations and to design new experiments thus, are very helpful for experimental chemistry. Theoretically predicted geometries, vibrational frequencies, bond dissociation energies, and other chemically important properties have become reliable enough to complement and sometime even to challenge the experimental data (Diedenhofen *et al.*, 2001).

Electronic structure theory is the application of quantum mechanics to calculate the structure and properties of molecules. Applying the principle of quantum mechanics to molecular properties is challenging in terms of exactly solving the Schrödinger wave equation. To solve the Schrödinger wave equation approximately various theoretical models have been developed. Understanding the strengths and weaknesses of these methods is the key for applications on target molecules. Determining factors in the choice of method includes the size of the molecules under study, and available computational resources. In this research, some computational methods have been used to determine the structural and chemical properties of all ligands and their complexes in order to gain more information about the properties of these compounds.

1.3.1 The Uses of Computational Chemistry

Computational chemistry is used in a number of different ways. One particularly important way is to model a molecular system prior to synthesizing the target molecule in the laboratory. Although computational models may not be precisely accurate, but they are often good enough to rule out 90% of possible compounds as being unsuitable for their intended use (Young, 2001). This is very useful information because synthesizing a single compound may require months of labor, raw materials cost and also generate toxic waste. A second use of computational chemistry is in understanding a problem more completely. There are some properties of a molecule such as electronic charge distribution, dipoles and vibrations frequency that can be obtained computationally more easily than by experimental means. There are also insights into molecular bonding, which can be obtained from the results of computations that cannot be obtained from any experimental method (Young, 2001).

1.3.2 The Tools of Computational Chemistry

At present, *ab initio* methods, density functional theory (DFT), molecular mechanics, and semi-empirical methods serve as the major computational tools of quantum chemistry. There is a trade-off between accuracy and computational effort in these methods. The most accurate results are obtained from high-level *ab initio* calculations with extended basis sets. Such calculations require the highest computational efforts and are extremely expensive for large molecules containing transition metal elements. On the other hand, semi-empirical calculations are fast, but of a limited reliability. Actual applications have to balance the required accuracy against the available computational resources. The combine use of several computational tools may well be the best approach to solve a given chemical

problem by performing initial explorations at the semi-empirical level followed by density functional and (if possible) high-level *ab initio* calculations (Deeth, 2003).

The main tools available belong to five broad classes as described below:

(i) Molecular mechanics (MM) is based on a model of a molecule as a collection of balls (atoms) held together by springs (bonds). If we know the normal spring lengths and the angles between them, and how much energy it takes to stretch and bend the springs, we can calculate the energy of a given collection of balls and springs, i.e. for a given molecule. Molecular mechanics is fast (Lewars, 2004).

(ii) *Ab initio* calculations (*ab initio* is from the Latin: "from first principles") are based on the Schrödinger equation. It is one of the fundamental equations of modern physics and describes among other things, how the electrons in a molecule behave. The *ab initio* method solves the Schrödinger equation for a molecule and gives us the molecule's energy and wavefunction. The wavefunction is a mathematical function that can be used to calculate the electron distribution (and, in theory at least, anything else about the molecule). From the electron distribution we can comment about the polarity of, and which parts of it are likely to be attacked by nucleophiles or electrophiles. The Schrödinger equation cannot be solved exactly for any molecule with more than one electron. Thus approximations are used; the less serious these are, the "higher" the level of the *ab initio* calculation is said to be. Regardless of its level, an *ab initio* calculation is based only on basic physical theory (quantum mechanics) and is in this sense "from first principles". *Ab initio* calculations are relatively slower compare to DFT and semi-empirical calculations (Lewars, 2004).

(iii) Semi-empirical calculations (SE) are, like *ab initio*, based on the Schrödinger equation. However, more approximations are made in solving it and the very complicated integrals that must be calculated in the *ab initio* method are not actually

evaluated in SE calculations: instead, the program draws on a kind of library of integrals that was compiled by finding the best fit of some calculated entity like geometry or energy (heat of formation) to the experimental values. This plugging of experimental values into a mathematical procedure to get the best calculated values is called parameterization. It is the mixing of theory and experiment that makes the method "semi-empirical". In other words, the semi-empirical method is based on solving the Schrödinger equation, but the equation is parameterized with experimental values (empirical means experimental). Semi-empirical calculations are slower than MM but much faster than *ab initio* calculations. SE calculations take roughly 100 times as long as MM calculations, and *ab initio* calculations take roughly 100-1000 times as long as SE (Lewars, 2004) .

In this research, semi-empirical methods, PM6 and ZINDO/S were used. These methods are described below:

The Zerner's INDO method (ZINDO) is also called spectroscopic INDO (INDO/S). This is a reparameterization of the INDO method specifically for the purpose of reproducing electronic spectra results. This method has been found to be useful for predicting electronic spectra. ZINDO is also used for modeling transition metal systems since it is one of the few methods parameterized for metals. It predicts UV transitions well, with the exception of metals with unpaired electrons. However, its use is generally limited to the type of results for which it was parameterized. ZINDO often gives poor results when used for geometry optimization (Young, 2001).

Charge transfer (CT) bands in non-solvatochromic systems and d-d transitions are particularly well reproduced. The oscillator strengths calculated using the dipole length approximation at the configuration interaction singles (CIS) level are usually overestimated by a factor of 2-3. The INDO/S calculations with the random-phase

approximation produce more accurate transition intensities. Solvent effects on absorption spectra can be estimated by using the self-consistent reaction field (SCRF) method or other approaches. ZINDO/S is available in Gaussian, HyperChem, ZINDO and CNDO/INDO semi-empirical packages (Gorelsky, 2003).

The semi-empirical method PM6 was designed primarily for the investigation of molecular species of biochemical interest. That is, the objective of parameter optimization was to reproduce the properties of molecules (Stewart, 2008). PM6 is the latest parameterization of the neglect of diatomic differential overlap (NDDO) method. Three modifications to the approximations have been made, these mainly affect the way the core-core interaction is defined. Parameters have been optimized for most elements, the exceptions being 12 of the lanthanides and all of the actinides (Stewart, 2007). The accuracy of PM6 in predicting heats of formation for compounds of biochemistry is somewhat better than Hartree-Fock (HF) or Becke, three-parameter, Lee-Yang-Parr (B3LYP) DFT methods, using the 6-31G(d) basis set (Stewart, 2007). Puzyn *et al.* strongly recommend that Quantitative structure-property relationship (QSPR) studies are carried out with PM6 and RM1 descriptors instead of the much more expensive DFT descriptors. The use of semi-empirical descriptors will allow the researchers to obtain QSPR models for thousands of new chemicals. These models are of similar quality to DFT-based models but can be built in a relatively short time (Puzyn *et al.*, 2008). Semi-empirical PM6 calculations were performed to better understand the origin of the photoluminescence. For example Roof *et al.* used PM6 to explain the photoluminescence of La_2KNbO_6 . These calculations provide a model for the HOMO–LUMO separation and explain the presence of an isolated state within the electronic structure of the compound, which is responsible for the intense blue-violet emission. It is well-known that orbital

energy differences strongly overestimate actual excitation energies, and either configuration interaction or time dependent treatments are needed to model the energetics of the electronic excitations. Nevertheless, the orbital energies provide a useful qualitative description (Roof *et al.*, 2008).

(iv) Density functional calculations [also called density functional theory (DFT) calculations] are, like *ab initio* and SE calculations, based on the Schrödinger equation. However, unlike the other two methods DFT does not calculate a wavefunction, but rather derives the electron distribution (electron density function) directly. In DFT, "functional" is a mathematical entity related to a function. Density functional calculations are usually faster than *ab initio*, but slower than SE. DFT is relatively new (serious DFT computational chemistry goes back to the 1980' s, while computational chemistry with the *ab initio* and SE approaches was being done in the 1960s) (Lewars, 2004).

(v) Molecular dynamics calculations apply the laws of motion to molecules. Thus one can simulate the motion of an enzyme as it changes shape on binding to a substrate, or the motion of a swarm of water molecules around a molecule of solute (Lewars, 2004).

1.4 Background and Literature Review for Schiff Bases

1.4.1 Definition

Schiff's bases, named after the German chemist Hugo Schiff (1834-1915) are those compounds having a formula $RR'C=NR''$ where R is an aryl group, R' is a hydrogen atom and R'' is either an alkyl or aryl group. However, usually compounds where R'' is an alkyl or aryl group and R' is an alkyl or aromatic group are also counted as Schiff bases (Layer, 1963; Daintith, 2000). The Schiff base class is very versatile as compounds can have a variety of different substituents and they can be unbridged or *N,N'*-bridged. Most common Schiff bases have NO or N_2O_2 -donor atoms but the oxygen atoms can be replaced by sulfur, nitrogen, or selenium atoms (Garnovskii *et al.*, 1993).

1.4.2 Preparation of Schiff Bases

Condensation between aldehydes and amines is realized in different reaction conditions, and in different solvents. The presence of dehydrating agents normally favors the formation of Schiff bases. $MgSO_4$ or Na_2SO_4 are commonly employed as a dehydrating agent. The water produced in the reaction can be removed azeotropically from the equilibrium using a Dean-Stark apparatus, when conducting the reaction in toluene or benzene. Primary alcohols like ethanol have been widely used as a solvent for the preparation of Schiff bases. Chromatography of Schiff bases on silica gel can cause some degree of decomposition of the Schiff bases, through hydrolysis. In this case, it is better to purify the Schiff base by crystallization methods. If the Schiff bases are insoluble in hexane or cyclohexane, they can be purified by stirring the crude reaction mixture in these solvents, sometimes adding a small portion of relatively polar solvent e.g diethyl ether and dichloromethane, in

order to eliminate impurities. In general, Schiff bases are stable solids and can be stored without many precautions (Cozzi, 2004).

1.4.3 Reaction Mechanism

The formation of Schiff base is catalyzed by dilute acid. Ideally the Schiff base formation takes place smoothly between pH 3-5. Deviation from this range of pH might affect the rate of reaction. The effect of acidity becomes clear when we consider that the loss of water from the carbinolamine is an elimination reaction which catalyzed by acid, Fig. 1.2. Furthermore the dehydration is the rate-determining step of the two step sequence. Since dehydration is acid-catalyzed, it seems clear that an increase in acidity should result in an increase in the rate of dehydration and thus in the rate of reaction. The amine is nucleophilic owing to the unshared pair of electrons on nitrogen. As the acidity of reaction medium increases, the amine is protonated and becomes non nucleophilic. Addition to the carbonyl group no longer takes place. The reaction is a balance between two steps which depend upon pH in opposite ways. Therefore, the reaction requires a careful control of pH. The solution must be acidic enough that some carbonyl groups are protonated, but not so acidic that all of the amino groups are protonated. At higher acid concentration, all the amine molecules are in the non-reactive protonated form. At the other extreme of low acid concentration, none of the carbonyl compound is in the reactive protonated form. In between these two extremes is the optimum pH (about pH 3-5) at which the rate of reaction is greatest. At this pH, some of amines are protonated, but some are free. Although most of the carbonyls compound are free, some are protonated and susceptible to attack (Pine, 1987; Fessenden and Fessenden, 1990; Borisova *et al.*, 2007).

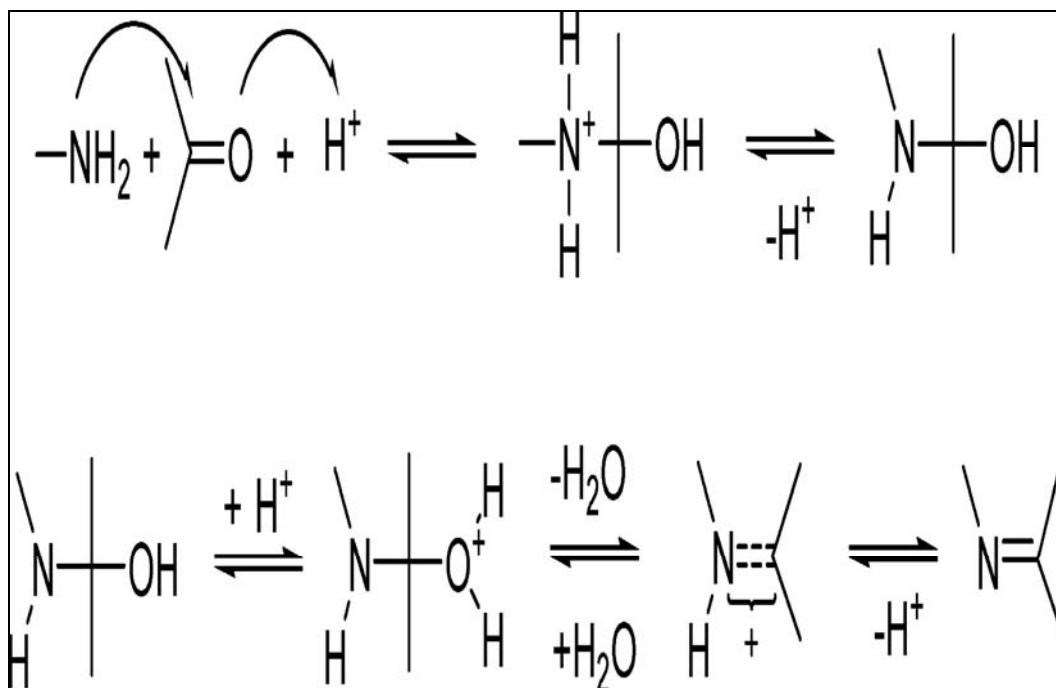


Fig. 1.2. Mechanism of condensation of carbonyl compounds with amines (Borisova *et al.*, 2007).

1.4.4 Schiff Base as Coordinating Ligands

Schiff base ligands coordinate to a metal through the imine nitrogen and another group, usually oxygen, situated on the original aldehyde. When a diamine was first combined with two equivalence of salicylaldehyde, the ligands came into being. The ligands feature two covalent and two coordinate covalent sites situated in a planar array. This makes the ligands ideal for the equatorial coordination of transition metals, leaving the two axial sites open for ancillary ligands. They are very much like porphyrins in this regard, but unlike porphyrins the Schiff base ligands are easy to prepare and are relatively inexpensive. Schiff bases are among the most general N ligands, because the basicity of the sp^2 -hybridized N lone pair, although lower than that of amines (sp^3 hybridization), is well suited to form complexes with metal ions. The salicylidene imine group is prone to undergo an acid-catalyzed hydrolysis, reverting to the corresponding salicylaldehyde and diamine in the presence of water. However, the stability of the Schiff base group increases considerably upon

coordination with a metal ion and formation of the Schiff base-metal complex. For this reason, in contrast to the free ligand, the Schiff base-metal complex can be used in wet solvents or even in aqueous media without undergoing hydrolysis (Baleizao and Gracia, 2006). Evidence for the tremendous amount of transition-metal chemistry that has been conducted is demonstrated by the fact that the first review in this area was published in 1966 (Holme *et al.*, 1966). By incorporating additional groups around the phenol portion of the ligand, such as *tert*-Butyl, the ligands can be made highly soluble in aromatic and aliphatic solvents. Incorporation of hydrophilic groups may also lead to ligands that are soluble in water and alcohols (Atwood and Harvey, 2001).

1.4.5 Applications of Schiff Bases and Their complexes

Schiff bases and their complexes have a wide variety of applications. They are useful in biological field, as anticancer (Popp, 1961; Popp and Kirsch, 1961), as antitumor (Hodnett and Moony, 1970), as antituberculous (Merchant and Chothia, 1970), as antimalarial (Ziegler *et al.*, 2000; Goldberg *et al.*, 1997, Sharma and Piwnca-Worms, 1999) and also they are found to have clinical, therapeutic (Argentini *et al.*, 1998) and analytical applications (Mo and Ogorevc, 2001). Earlier work has shown that some drugs showed increased activity when administered as metal chelates rather than organic compound (Raman *et al.*, 2001).

The malleability inherent to the Schiff base ligands has led to their extensive use in transition-metal chemistry, particularly in modeling enzymes and in catalysis (Jacobsen, 1993). More recent applications include use as metal containing liquid-crystalline polymers (Serrano and Oriol, 1995), as non-radioactive models for Technetium (van Bommel *et al.*, 1998), as antiviral agents (Takeuchi *et al.* 1999;

Louie and Meade, 1998), as chiral phase-transfer catalyst (O'Donnell, 2004), and also in asymmetric catalysis (Canali and Sherrington, 1999; Jacobsen, 2000).

Schiff bases are suitable ligands for the preparation of libraries due to the easy reaction conditions. Variety of chiral amines and aldehydes are used as precursors to synthesize Schiff bases. Amino acids and peptides are particularly suitable for the creation of effective catalysts. The condensation of aldehyde-bearing coordinating groups with amino acids and peptides provide interesting Schiff bases, used to make a combinatorial library of ligands (Cozzi, 2004).

1.5 Background and Literature Review for Zinc Complexes

Complexes of transition and non-transition metals with Schiff base ligands are promising materials for optoelectronic applications due to their outstanding photoluminescent and electroluminescent properties, and the ease of synthesis that readily allows structural modification for optimization of material properties. Metal complexes offer many attractive properties, such as displaying a double role of electron transport and light emission, higher thermal stability, and ease of sublimation. Moreover, an attractive feature of these complexes is the ability to generate a much greater diversity of tunable properties and their color emission by virtue of the coordinated metal center or by modifying the backbone substituents of ligands (Yu *et al.*, 2008).

Zinc is an essential trace element and the second most abundant transition metal after iron in the body. There has long been an interest in the synthesis of zinc complexes, due to its unique physical, chemical, catalytic and optical properties.

The interest in zinc from the chemist's view stems from its unique properties. The most important properties of zinc are stable oxidation state Zn(II), lack of redox

chemistry, the flexibility in coordination number and geometry, and the Lewis acidity which is the key to its catalytic roles (Archiblad, 2003).

Zinc complexes of Schiff base became attractive for their interesting fluorescent properties, in particular, the salicylideneamine-Zn(II) complexes exhibit photoluminescence as well as electroluminescence (Yu *et al.*, 2008). Zinc(II) complexes are especially attractive for spectroscopic investigations of coordinated ligands because the spectra of these compounds are not complicated by ligand field bands or low-energy charge-transfer transitions involving the d^{10} metal center.

1.5.1 Coordination Geometry of Zinc Complexes

Coordination numbers of zinc are most commonly four to six, with three not quite so common, and two, seven and eight less often observed and more dependent on donor or ligand types. Distorted tetrahedral, five-coordinate geometries and octahedral are frequently observed geometries. The Cambridge Structural Database contains a large number of square planar complexes due to the vast array of porphyrin and related ligand systems structurally characterized with zinc (Archiblad, 2003).

A coordination number of two is mainly observed with amide, silyl, and alkyl donors. Extremely bulky thiophenolate and selenophenolate complexes of zinc also show structurally characterized two-coordinate zinc centers, with an S_2 or Se_2 donor set. Trigonal planar geometry is more common for zinc especially with alkyl, amide, and bulky phenolate and thiophenolate ligands. Dimeric or larger species can be formed and trigonal geometry is very much dependent on the steric bulk of the ligands. Trigonal-pyramidal geometry has been observed for zinc with an appropriately restricted ligand. Square planar zinc is most often observed in porphyrin and phthalocyanine complexes where the ligand restricts the binding geometry. Examples of square planar geometry with oxygen are rare. Higher coordination numbers of

seven and eight are unusual for zinc. The flexibility of coordination geometry and number is important in solution as well as in the solid state and leads to equilibria of species with different coordination numbers. Of particular interest is the coordination environment of zinc in proteins and the preference for tetrahedral or octahedral geometry. Four-coordinate zinc plays a structural role in zinc finger proteins and enzymes (Archiblad, 2003).

1.5.2 Zinc in Biology

Zinc always occur as a divalent cation Zn(II) in biological systems, it is the second most abundant transition metal next to iron. Zinc containing compounds are useful model compounds for biochemical research, as zinc(II) plays an important role in several zinc-containing metal enzymes such as zinc-peptidases (Rees *et al.*, 1983; Lee *et al.* 1998), human carbonic anhydrase (Silverman and Lindskog, 1988) and alkaline phosphatase (Kim and Wyckoff, 1991).

Although the majority of biological zinc ions are tightly sequestered by proteins , the presence of “free zinc pools” in certain cells may still be possible. The most important and best known role for zinc is as a structural cofactor in metalloproteins. Over the last few decades, hundreds of zinc proteins possessing one or more zinc-stabilized motifs have been identified and classified into several major families. Meanwhile, zinc(II) ions are directly associated with the regulation of gene expression through metalloregulatory proteins such as metal-response element-binding transcription factor-1 that acts as a cellular zinc sensor. In addition, zinc(II) ions are also present in most DNA or RNA polymerases (Jiang and Guo, 2004).

1.5.3 The Photophysical Properties of the Schiff Base-Zn(II) Complexes

Luminescent metal complexes are key materials for several applications such as lighting, analytical probes, and lasers. In many cases compounds based on precious metal like platinum and rare earth metals are utilized, which are often rather expensive and non-environmental friendly. In recent years, interest is growing in luminescent complexes based on less traditional but more abundant and cheaper metal elements. In this scenario compounds of metals with a d^{10} electronic configuration are playing a prominent role, also thanks to the versatility of their luminescent levels which can be of ligand centered, charge transfer or in the case of polynuclear compounds, even metal-centered nature (Barbieri *et al.*, 2008).

It has been shown that some d^{10} metal complexes with N,O-donor ligands demonstrate excellent emitting properties. Among them, Zn(II) complexes have proven to be important emitters for their excellent emitting properties and low cost, in comparison with other d^{10} metal e.g. Au(I) complexes (Tong *et al.*, 2005).

In 1993, Hamada and his coworkers pioneered Schiff base-Zn(II) complexes as blue to greenish-white emitters for electroluminescence devices. They concluded that the electroluminescence cells with azomethine-zinc complexes showed a bright blue emission. These emission peaks were in the 458-470 nm range. The azomethine-zinc complexes exhibited good electron transport capability, as indicated by the high luminescence obtained in two-layer electroluminescence cells (Hamada *et al.*, 1993).

In 1996, Hamada and his group, synthesized four chelate-metal complexes bis[2-(2-hydroxyphenyl)benzoxazolate]zinc, bis[2-(2-hydroxyphenyl)benzothiazolate]zinc, bis[2-(2-hydroxynaphtyl)benzothiazolate]zinc and bis[2-(2-hydroxyphenyl)3-octylbenzotriazolate]zinc, in order to obtain white-emitting material. These compounds

were fabricated as electroluminescence devices and they give emission in green, greenish-white, blue and orange region (Hamada *et al.*, 1996).

In 1996, two lumophores based on aluminum and zinc metallo-8-hydroxyquinolates have been prepared as electroluminescent materials, and their absorbance, photoluminescence, and electroluminescence properties were compared with unsubstituted versions of the same complexes. 8-Hydroxy-5-piperidinyl quinolinesulfonamide was synthesized in order to add an electron-withdrawing substituent at 5-position in 8-hydroxyquinoline, increasing the solubility of the corresponding metal quinolate complexes in non-polar solvents, and producing a blue-shift in the emission wavelength maximum, relative to complexes formed from the unsubstituted compound (Hopkins *et al.*, 1996).

Many Zn(II) complexes are known to exhibit intense fluorescence at room temperature and there has been substantial research assessing the performances of Zn(II) complexes in fluorescence-based OLED devices (Sano *et al.*, 2000). The fluorescence emission stems from a π - π^* ligand-centred transition and the role of the central atom is to provide stability to the ligand. The modification of the ligand often leads to a change of emission energy, emission intensity and stability of the complex, along with a dramatic change of the structure and bonding (Hamada *et al.*, 1996).

In 2003, Yu *et al.* revealed the structure of the white-emitting electroluminescent material, Bis[2-(2-hydroxyphenyl)benzothiazolate]Zn(II) [Zn(BTZ)₂] is one of the best white electroluminescent materials used in organic light-emitting diodes (OLEDs). The structure of the chelate is dimeric [Zn(BTZ)₂]₂ with two isotropic Zn(II) ion centers having five-coordinate geometry. Strong intermolecular interaction may be expected to enable good electron transport properties as compared with tris(8-hydroxyquinolinato)aluminum (Yu *et al.*, 2003).

Phosphorescence from Zn(II) complexes are generally observed only in low-temperature glasses. Two blue phosphorescent Zn(II) complexes have reported emission in solid state at room temperature (Liu *et al.*, 2004). The emission is assigned to a $^3\text{IL } \pi\text{-}\pi^*$ state, due to the long excited state lifetime.

Several Zn(II) complexes such as bis[8-hydroxyquinoline]Zn(II), bis[2-(2-hydroxyphenyl)pyridine]Zn(II), bis[2-(2-hydroxyphenyl)-5-phenyl-1,3,4-oxadiazole]Zn(II), bis[2-(2-hydroxy phenyl)-5-phenyl-1,3,4-thiadiazole]Zn(II) and bis[2-(2-hydroxyphenyl)thiazole]Zn(II) have been reported as potential OLED materials. However, each of these complexes has certain drawbacks when used for a practical OLED device (Kim *et al.*, 2003).

Tong *et al.* reported syntheses, crystal structures, and luminescence properties of two neutral, monomeric Zn(II) complexes with benzimidazole derivatives, namely Zn[2-(2-hydroxyphenyl)benzimidazole]₂ and Zn[5-amino-2-(1*H*-benzimidazol-2-yl)phenol]₂. The electronic transitions in the photoluminescent process have also been studied by means of time dependent density functional theory (TDDFT) calculations (Tong *et al.*, 2005).

In 2006 Ghosh *et al.*, reported the synthesis, structure and photophysical behavior of two different Zn(II) complexes with hexa- and penta-coordination environments of the metal centre. The structural analyses revealed that each zinc atom is dinuclear, has distorted trigonal bipyramidal geometry with a ZnN₅ chromophore. Whereas, in molecular ion-pair, the Zn(II) ion has a distorted octahedral environment in the cationic part with a ZnN₆ chromophore and the remaining Zn(II) ion in the anionic part has a distorted tetrahedral geometry with a ZnN₄ environment. All the complexes display intraligand fluorescence and intraligand phosphorescence in glassy solutions (Ghosh *et al.*, 2006).

In 2007, an aromatic Schiff base ligand, *N, N'*-bis[(4, 4'-diethylamino)salicylidene]-1, 2-phenylenediamine and its trinuclear Zn(II) complex were synthesized. The complex exhibited blue-green emission as the result of the fluorescence from the intraligand emission excited state (Yu *et al.*, 2007a).

In 2007, Yu *et al.*, reported a zinc complex containing oxa-alkyl chain and naphthols were synthesized and investigated for OLEDs. The ZnL complex exhibited strong blue fluorescence and good thermal stability and also was easily made in uniform thin films in vacuum vapor deposition. OLEDs based on the complex showed a strong blue emission at 455 nm. The results revealed that the flexible chain-having Schiff base complexes are advantageous over the aromatic bridged ones in solubility as well as processability for OLEDs. A proper design of the metal ions and the ligands synthesized from a heteroatom alkyldiamine and a conjugated aromatic aldehyde is important to achieve high stability and excellent electroluminescence characteristics (Yu *et al.*, 2007b).

Kawamoto and his coworkers reported that the synthesis of Zn(II) complexes with 2-substituted benzothiazolines afforded tetrahedral mononuclear complexes, [Zn(R-Ph-C(H)=N-C₆H₄-S)₂] with a N₂S₂ donor set. Zn(II) in a distorted tetrahedral geometry. It has been found that the electronic properties of the substituents, as well as their positions on the pendent phenyl rings of the Schiff base ligands affect the electronic absorption spectra of the complexes. All the complexes were luminescent in CH₂Cl₂/toluene glass at 77 K (Kawamoto *et al.*, 2008).

Quantitative analysis of trace metal ions with a selective analytical reagent has gained considerable importance in environmental and biological applications. Remarkable developments of fluorescent indicators have been made for biologically important divalent metal ions. Zn(II) ion has been recognized as an important cation